PCCP

ROYAL SOCIETY OF CHEMISTRY

PAPER

View Article Online
View Journal | View Issue

Cite this: *Phys. Chem. Chem. Phys.*, 2024, **26**, 12510

Bridging the gap: viable reaction pathways from tetrahedrane to benzyne†

Taylor A. Cole, Steven R. Davis, Athena R. Flint and Ryan C. Fortenberry *

Received 20th December 2023,
Accepted 5th April 2024

DOI: 10.1039/d3cp06199j

rsc.li/pccp

The addition of sp-carbon-containing molecules to polycyclic sp^3 tetrahedrane (*c*-C_4H_4) results in the formation of both *o*-benzyne (*c*-C_6H_4) and benzene (*c*-C_6H_6). Since both *c*-C_6H_4 and *c*-C_6H_6 have been detected in the interstellar medium (ISM), providing additional pathways for their possible astrochemical formation mechanisms can lead to the discovery of other molecules, such as *c*-C_4H_4, benzvalyne, and vinylidene (:CCH_2). Addition of diatomic carbon (C_2), the ethynyl radical (C_2H), vinylidene, and acetylene (HC≡CH) to *c*-C_4H_4 is undertaken in individual pathways through high-level quantum chemical computations at the CCSD(T)-F12b/cc-pVTZ-F12 level of theory. The resulting C_2 addition pathway proceeds barrierlessly through benzvalyne as an intermediate and reaches a true minimum at *c*-C_6H_4, but no leaving groups are produced which is required to dissipate excess energy within an interstellar chemical scheme. Similarly, the C_2H addition to *c*-C_4H_4 produces benzvalyne as well as its related isomers. This pathway allows for the loss of a hydrogen leaving group to dissipate the resulting energy. Lastly, the HC≡CH and :CCH_2 addition pathways follow through both benzvalene and benzvalyne in order to reach *c*-C_6H_6 (benzene) and *c*-C_6H_4 (*o*-benzyne) as well as H_2 as the required leaving group. Although there is a barrier to the HC≡CH addition, the :CCH_2 addition presents the contrary with only submerged barriers. These proposed mechanisms provide alternative possibilities for the formation of complex organic molecules in space.

1 Introduction

Hydrocarbons are known to exist in the interstellar medium (ISM)[1,2] with polycyclic aromatic hydrocarbons (PAHs) potentially responsible for around a quarter of the carbon molecularly sequestered in the ISM.[3] Recent research confirms that PAHs are the primary precursors to soot particles,[4] showcasing that these molecules are broadly applicable and not just limited to astrochemistry. This narrative enriches our comprehension of PAHs and underscores their universal presence and significance, both in earthly and cosmic environments. Their aromatic nature and relation to recently detected molecules in the ISM[1,2,5,6] promote their discussion in current astrochemical conversations.[7,8] As the astrochemical significance of PAHs increases, understanding their involved precursors and reaction pathways are crucial for a full picture of the organic and prebiotic chemistry of the ISM.

Many cyclic hydrocarbons, such as *c*-C_6H_6 (benzene)[9,10] and *c*-C_6H_4 (*o*-benzyne),[6] have been detected toward various astronomical regions, and their existence opens the possibility for new chemistry to be explored. Several C_6H_4 isomers lie along the potential energy surface between low-energy aromatic structures. One example is benzvalene, which was first synthesized *via* photochemical reactions of *c*-C_6H_6 in the laboratory nearly 60 years ago.[11] Other studies delve into the potential mechanisms relating *c*-C_6H_6 to *c*-C_6H_4 and their additional isomers and derivatives.[12,13] This research provides a possible foundation for how such reactions could take place in the gas phase with astrochemical applications clearly in view. Resulting reaction intermediates could serve as possible targets for the QUIJOTE[1] or GOTHAM line surveys and the exploration of PAHs in molecular clouds, such as TMC-1.[14–20] Beyond PAHs and their related species, other notable sources of carbon in the universe include C_2 and its hydrogenated C_2-containing affiliates, such as C_2H (ethynyl radical), HC≡CH (acetylene), and :CCH_2 (vinylidene).[21–24] The diatomic carbon molecule (C_2) has been detected in the near IR spectrum of Cyg OB2 No. 12,[21] and HC≡CH has been previously detected in the IR spectrum of IRC +10° 216, and molecular clouds GL 2591, W3 1RS 5, and OMC-1 IRc2.[23,24] :CCH_2 is reported to have strong IR intensities for the ν_1 CH symmetric stretching at 3025 cm^{-1}, ν_2 C=C stretching at 1635 cm^{-1}, ν_3 CH_2 scissoring at 1165 cm^{-1}, and ν_6 CH_2 rocking at 450 cm^{-1}.[25–27] Although the :CCH_2 isomer has not been detected, its strong vibrational intensities

Department of Chemistry and Biochemistry, University of Mississippi, University, Mississippi, 38677, USA. E-mail: r410@olemiss.edu

† Electronic supplementary information (ESI) available: Containing cartesian coordinates for all geometric structures. See DOI: https://doi.org/10.1039/d3cp06199j

provide potential for identification. These hydrocarbons could contribute materials to support complex chemistry and the creation of variable organic structures in the ISM since small molecules like C_2 can become potential building blocks for the formation of c-C_6H_6 and other, more complex, PAHs.[28] The growth of such chemistry through the interaction of these molecules may help to provide insights into astronomical spectral observations that have eluded explanation for decades.

Most notably, the unidentified infrared bands (UIRs) are spectral features that have not been definitively linked to any certain molecule to date and are observed in the infrared region of the electromagnetic spectrum toward various astronomical objects.[29–32] They were first reported from observations of the planetary nebulae NGC 7027, BD + 30° 3639, and NGC 6572.[33] The current hypotheses suggest PAHs as contributing factors to these spectral lines with a possible inclusion of their aliphatic counterparts or mixed aliphatic-aromatics hydrocarbons.[34–39] Beyond the infrared, ultraviolet wavelengths may also be applicable to PAHs. In 1965, a 2175 Å ultraviolet extinction bump was discovered in the ISM[40] and further supported by the Orbiting Astronomical Observatory 2.[41] Observations of this so-called ''UV-Bump'' have since shown this feature to be widespread and distinct in the Milky Way Galaxy.[42] Similarly to the UIRs, this interstellar extinction bump has no known current rationale that explains its existence. However, some speculation as to its provenance includes carbonaceous molecules and PAHs.[43–45]

One such hypothesis for the origin of the UV-Bump is that of carbonaceous molecular clusters exhibiting a T-carbon molecular structure in which the vertices of a cubic diamond lattice are replaced with a tetrahedral arrangement of carbons. Such an sp^3 carbon motif is theorized to be responsible for at least part of the UV-Bump.[46] Considering the abundance of neutral hydrogen in the interstellar cosmos,[47,48] T-carbons may exist in a hydrogenated form with 40 carbon and 16 hydrogen atoms, subsequently denoted as hydrogenated T-carbons (HTCs). The variable sizes of carbonaceous molecules and clusters in interstellar dust[49] may enable HTCs to exist as a mixture of clusters. These HTCs produce a striking absorption peak at roughly the same wavelength as the extinction bump. Then, when combined with other hypothesized molecular clusters such as graphite, $MgSiO_3$, and Fe_2SiO_4, a well-fitted mixed model is obtained with startling correlation to the UV-Bump.[50] Whether HTCs contribute to this 2175 Å feature remains to be seen, but their role in the astronomical carbon budget has not been explored in as much detail as PAHs or their derivatives.

The main HTC molecular building block, c-C_4H_4 (tetrahedrane), has been subjected to intense research for years due to its high angle strain and kinetic stability. Unlike other platonic species, including cubane and dodecahedrane, tetrahedrane has been elusive in the synthesis process, fostering further research.[51–53] The uptick in attention towards increasingly complex hydrocarbons in interstellar environments has brought c-C_4H_4 some research attention due to its structural prominence and theorized implementation in larger, more complex molecules in the ISM.[54–56] This c-C_4H_4 aliphatic monomer has shown to be a minimum on a potential energy surface[57] and is likely stable in cold, low pressure environments, *i.e.* the ISM. More recently, its rovibrational data obtained from quartic force field calculations reveal two intense vibrational frequencies close in proximity to UIRs, providing possibility for detection in both the ISM and the laboratory.[58–60] Because of tetrahedrane's correlation with HTCs, UIRs, and the UV-Bump, further astrochemically-minded research into this organic molecule is warranted. Since c-C_4H_4 is so strained, reactions with simple, C_2-containing molecules could lead to the known interstellar molecule c-C_6H_4, and may have implication in the larger chemistry of PAHs.

A likely intermediate along the reaction pathway of c-C_4H_4 and C_2 is benzvalyne, another theoretical hydrocarbon. Previous work has shown this structure to be a minimum with a significant dipole moment of 2.6 D and formative correspondence to already-detected interstellar molecules like c-C_6H_4 along the reaction pathway.[12,13] Benzvalyne is shown to be a required intermediate between c-C_4H_4, c-C_6H_6, and c-C_6H_4 in a potential energy surface (PES) that links these species. This bicyclic isomer of c-C_6H_4 can offer an internal perspective for the pathways of sophisticated hydrocarbons in interstellar environments. Any correlation between these detected and undetected organic molecules can provide additional advantageous results for future detection signal acquisitions in the ISM and understanding of their overall chemistry. Hence, this work will explore reactions of c-C_4H_4 with C_2, C_2H, $HC{\equiv}CH$, and $:CCH_2$. While such reactions are believed to play an important role in astrochemistry, their role in combustion chemistry cannot be neglected as these molecules and their derivatives are known to inflict harmful consequences towards the climate, environment, and overall human health.[4,61–65]

2 Computational methods

The small size of the systems under study within this work allows for the use of highly-accurate quantum chemical methods to be employed. The current ''gold-standard'' method within computational chemistry is CCSD(T),[66–71] often paired with the cc-pV*X*Z basis sets of Dunning and coworkers.[72–74] The CCSD(T)/cc-pV*X*Z level of theory can be improved through the addition of an explicit-correlation (F12) correction for a negligible increase in computational cost.[75–79] The CCSD(T)-F12b/cc-pV*X*Z-F12 level of theory, through the inclusion of short-range interelectronic interactions, is shown to increase calculation accuracy significantly; addition of the F12 correction to the CCSD(T)/cc-pV*X*Z level of theory is shown to produce results of CCSD(T)/cc-pV(X + 2)Z accuracy.[80] Throughout this work, the primary level of theory will be CCSD(T)-F12b/cc-pVTZ-F12, hereafter abbreviated as F12-TZ.

All reactant, product, and intermediate structures are optimized, alongside harmonic frequency calculations, at the F12-TZ level of theory using the MOLPRO 2022.3 quantum chemical software.[81–83] Transition state structures are

optimized, followed by the requisite frequency calculations, at the B3LYP[84–88]/aug-cc-pVTZ[72,73,89] level of theory using the Gaussian16[90] software package. In order to correctly place these structures along the reaction pathway, a single-point energy calculation is done at the F12-TZ level of theory in MOLPRO at the B3LYP transition state optimized geometry, a method shown to work well for explaining observed, experimental reactions.[91,92] Intrinsic reaction coordinate (IRC) calculations[93] are performed at the B3LYP/aug-cc-pVTZ level of theory in Gaussian so that the computed transition states correspond to the desired motion along the reaction coordinate.

In some cases, the energy profile of the pathway may not be able to be described through a transition state, or a transition state structure may be difficult to locate. In such situations, a relaxed potential energy surface (PES) scan can be created in order to evaluate the potential surface more rigorously. Relaxed potential energy scans follow the variable corresponding to a given reaction coordinate, such as an interatomic distance or angle, by constraining the geometric variable to a series of values between two points of interest. At each value of this variable, the remainder of the structure is allowed to optimize around it. The electronic energies of each partially-constrained geometry along the coordinate can be plotted and used to visualize a two-dimensional slice of the potential energy surface. Points within each relaxed PES scan are optimized at the B3LYP/aug-cc-pVTZ level of theory, followed by single-point energy calculations at the F12-TZ level of theory, in MOLPRO.

In the addition of C_2H to *c*-C_4H_4, a PES is generated to model the change in energy as the terminal carbon of C_2H approaches a carbon vertex in *c*-C_4H_4. Points are created over a 1.0–4.0 Å interatomic range in increments of 0.1 Å. On the C_6H_6 potential surface, two PESs are constructed. One PES is created to visualize the change in energy as the angle between the migratory hydrogen of $TS1_a$ (see below) and the two terminal carbon atoms increases. Points for this scan are generated over a 30°–150° range in increments of 0.3°. The final PES scans over the distance between a carbon vertex in *c*-C_4H_4 and a dummy atom placed within the carbon–carbon bond of HCCH. The X–C reaction coordinate variable is varied over a 1.0–4.3 Å range in increments of 0.1 Å.

The PESs discussed above can reveal internal conversions between structures with differing orbital configurations.

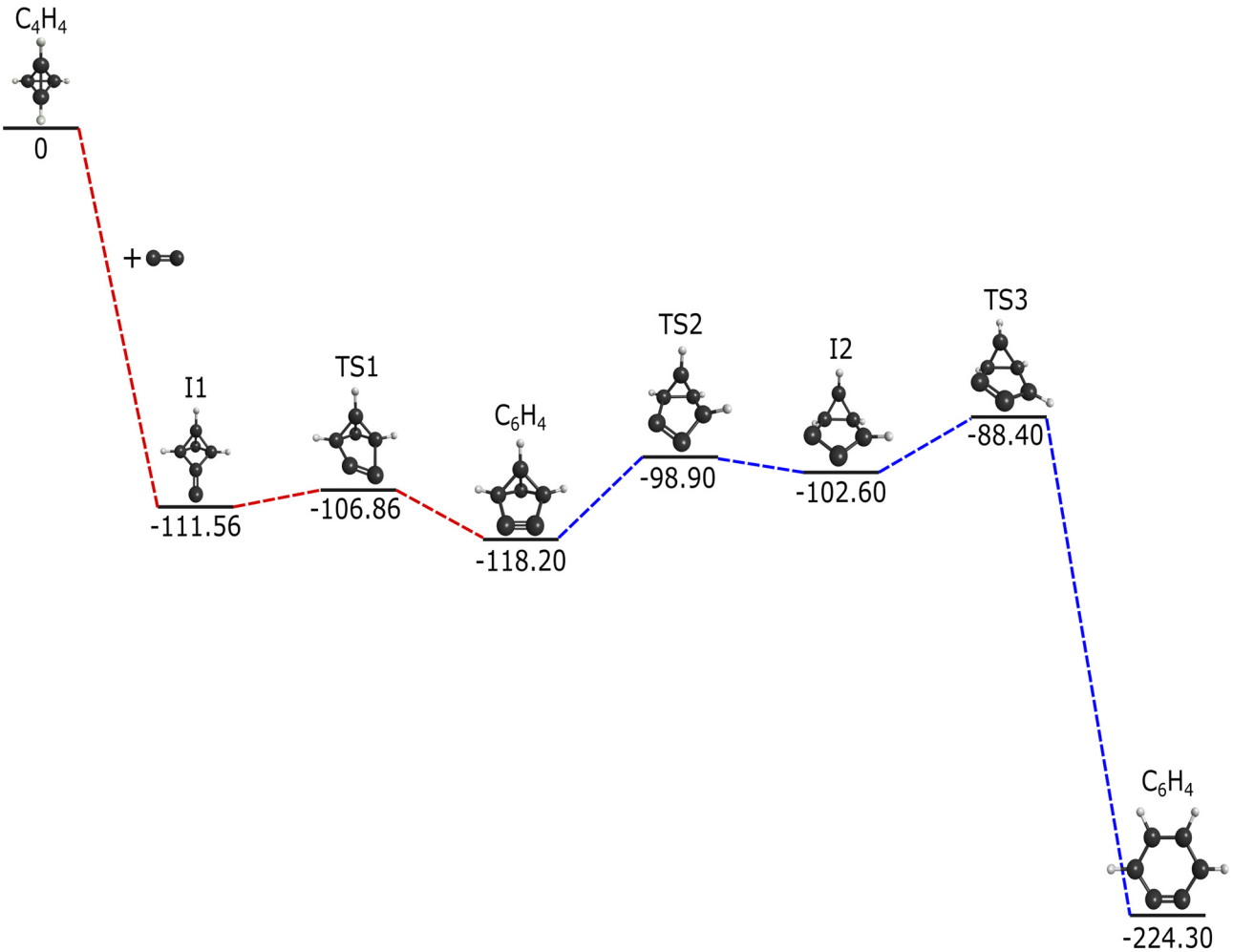

Fig. 1 Reaction pathway for the formation of *c*-C_6H_4 *via* C_2 addition to *c*-C_4H_4 in kcal mol^{-1}. Red dashed lines represent this research, and blue dashed lines from Poland *et al.*[12]

To visualize how the reaction proceeds through these internal conversions, correlation diagrams are created by plotting the frontier orbitals of structures before and after the internal conversion on the potential surface. Molecular orbital calculations on these structures are done at the RHF/aug-cc-pVTZ level of theory (for closed-shell references) or the ROHF/aug-cc-pVTZ level of theory (for open-shell references) with Gaussian16. Molecular orbital visualizations are created in Gabedit.[94,95]

3 Results and discussion

3.1 C_2 addition to *c*-C_4H_4

The addition of C_2 to *c*-C_4H_4 results in the reaction pathway given in Fig. 1. This reaction runs barrierlessly to an intermediate at −111.56 kcal mol^{-1} below the starting materials. This intermediate passes through a transition state with a small, 4.7 kcal mol^{-1} increase and settles at benzvalyne, −118.20 kcal mol^{-1} relative to the initial reactants.

The imaginary vibrational mode of TS1 has a frequency of 342.5*i* cm^{-1} and shifts the two foremost carbons back and forth, providing a connection between I1 and benzvalyne. The −118.2 kcal mol^{-1} decrease from the reactants implies that additional energy is available for further chemistry after this initial creation of benzvalyne. Also, benzvalyne has been shown to be a possible intermediate towards the creation of *c*-C_6H_4.[12] Due to these two factors, this previously-researched pathway included in blue in Fig. 1 in order to formulate the connection from benzvalyne to *c*-C_6H_4.[12] This additional route is recomputed to match the current level of theory and encompasses a multi-transition state barrier from benzvalyne. Benzvalyne, I1, and TS1 are all more than 100 kcal mol^{-1} lower than the reactants, providing the thermodynamics necessary for chemistry to take place in low-temperature and low-pressure environments. Additionally, the relatively low energy barriers from intermediates to TSs imply that the kinetics should also be favorable.

Alone, this reaction would not be feasible in the ISM or most low-pressure gas phase environments, unfortunately. When combined with the reactive steps stemming from *c*-C_4H_4 and C_2, an overall favorable reaction mechanism is formed. Notably, *c*-C_6H_4 is −224.3 kcal mol^{-1} lower than the combination of *c*-C_4H_4 and C_2. However, since no leaving group is present that would result in isolation of *c*-C_6H_4, this formation pathway is less feasible.[96,97] While radiative stabilization of *c*-C_6H_4 is possible in theory, such processes have yet to be observed experimentally for neutral–neutral reactions.[98] As procession through an available bimolecular exit channel, if it exists, is often much faster than the corresponding radiative stabilization process for small species,[99] *c*-C_6H_4 is more likely to redissociate into reactants or generate nontargeted products on this pathway.

Using the acquired information about the C_2 addition reaction pathway, there is potential for *c*-C_4H_4 to be a feasible reactant of the already-detected *c*-C_6H_4 if some form of a leaving group presents itself through additional reactive connections. However, the most natural place to expect a leaving group would come from the incident molecule and not the *c*-C_4H_4, making a hydrogen atom from the closely-related C_2H triatomic molecule[100] the next step for collisions with the present HTC standin utilized here, *c*-C_4H_4.

3.2 C_2H addition to *c*-C_4H_4

The supplemental hydrogen from the addition of C_2H, a molecule first detected in the Orion Nebula with the National

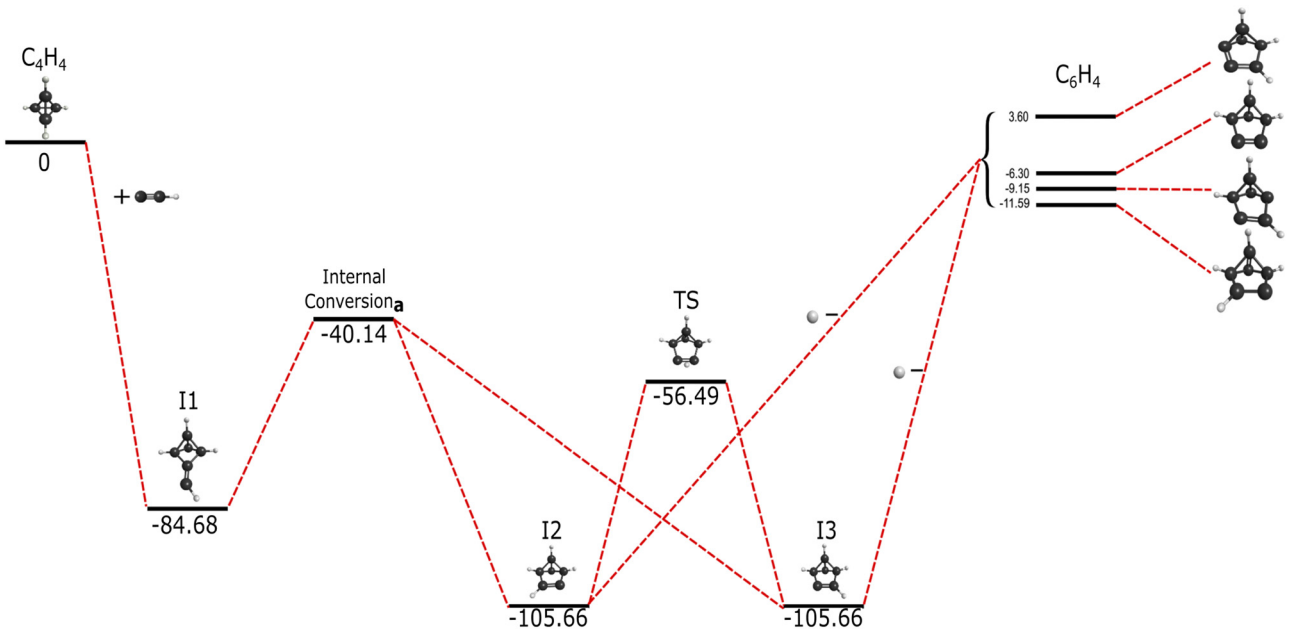

Fig. 2 Reaction pathway for the formation of benzvalyne *via* C_2H addition to *c*-C_4H_4 in kcal mol^{-1}. Internal conversion$_a$ represents the intersection seen in Fig. 3.

Radio Astronomy Observatory,[22] creates a unique reaction pathway in comparison to that of the addition of C_2. This reaction, present in Fig. 2, proceeds barrierlessly towards the first submerged-well intermediate, I1, at −84.68 kcal mol^{-1} relative to the reactants akin to the formation of I1 in Fig. 2. Similar organic molecules appear throughout these reaction pathways even if I1 in the C_2H addition is higher than I1 in the C_2 reaction. Both I1 structures in Fig. 1 and 2 are qualitatively equivalent in structure, but the additional hydrogen in the C_2H I1 creates an odd number of electrons, resulting in free radical behavior and thus increased reactivity. Intermediate I2 in Fig. 2 is also structurally similar to benzvalyne showcasing consistent behavior as would be expected for systems that only differ by a single hydrogen atom.

In contrast to the C_6H_4 potential surface described previously where a transition state separates I1 and benzvalyne, this C_6H_5 potential surface (where the ethynyl radical and tetrahedrane react) allows I1 and I2 to interconvert through an internal conversion of molecular structures as shown in the scan depicted in Fig. 3. This varied distance between the terminal carbon on the C_2H and a carbon on tetrahedrane produces two potential energy wells as described in Section 2 which cross when the distance reaches approximately 2.2 Å. This internal conversion can promote the radiationless interchange between structures of the same orbital symmetry.[101–104] While I1 and I2 appear to be structurally different, their orbital spaces are actually closely related. When observing the geometries closest to the exact point of conversion, the two highest-energy occupied molecular orbitals (HOMOs) and the lowest-energy unoccupied molecular orbitals (LUMOs) retain their original symmetry and ordering through this internal conversion as given in Fig. 4. While I1 represents a minimum, I2 is a lower energy isomer. The orbital topologies, ordering, and occupation remain consistent between I1 and I2 as shown in Fig. 4 on both sides of the internal conversion, but the

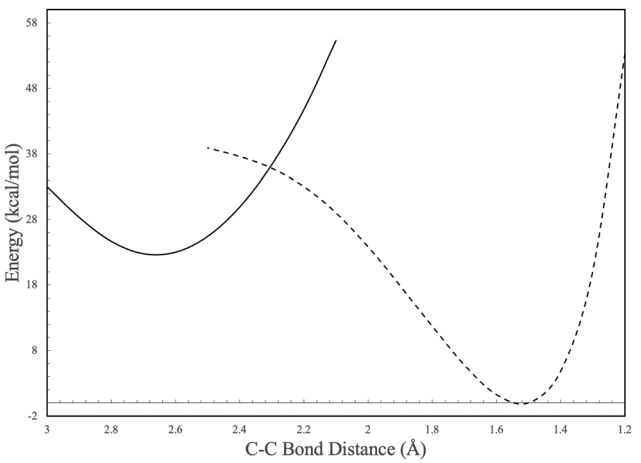

Fig. 3 Potential energy scan of the C–C bond between C_2H and c-C_4H_4. Solid and dashed lines represent individual molecular configurations correlating to I1 and I2 in Fig. 2.

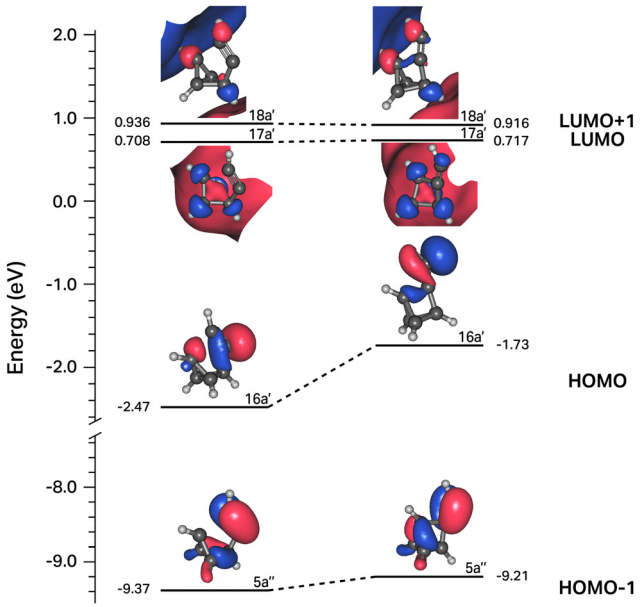

Fig. 4 Correlation diagram for the four frontier orbitals of structures to the right and left of the internal conversion shown in Fig. 3.

repositioning of the carbon atoms in I2 (to the right of the internal conversion in Fig. 3) optimizes the orbitals slightly differently and produces the lower-energy state. As such, the molecule can shift surfaces readily when the interacting carbon atoms are placed at roughly 2.2 Å from one another. This, of course, could be true for any tetrahedrane carbon as all are equivalent by symmetry.

Moving on to the relationship between I2 and I3 in Fig. 2, the connectivity and achirality of both I2 and I3 show that they are inherently the same molecule with the same energies and capabilities. As I2 at −105.66 kcal mol^{-1} isomerizes towards I3 through a transition state, either conformation can be created from I1, and both can expel a hydrogen atom as a leaving group.

The departure of the H atom from either I2 or I3 creates four different, bicyclic isomers of c-C_6H_6. Benzvalyne comes third in stability at −6.3 kcal mol^{-1} below the reactants, where two other C_6H_4 isomers lie lower at −9.15 kcal mol^{-1} and −11.59 kcal mol^{-1} as given in the upper-right of Fig. 1. In addition to these three, there is an additional isomer of C_6H_4 that lies above the reactants at 3.6 kcal mol^{-1} which is unlikely be accessed in the gas phase as it will be higher in energy than the reactants and would require more than 1600 K in ambient temperature. The transition state energies for the interconversion between these isomers creates a further thermodynamic barrier as they are dozens of kcal mol^{-1} above the reactants' energy. Hence, once these isomers are made in the gas phase, they cannot interconvert between one another if they are formed in this pathway. The likely Boltzmann behavior for the distribution of these isomer populations implies that benzvalyne will still be able to contribute to the formation of *o*-benzyne, but it will not be the dominant player. Other reactions would be able to contribute moreso to their populations.

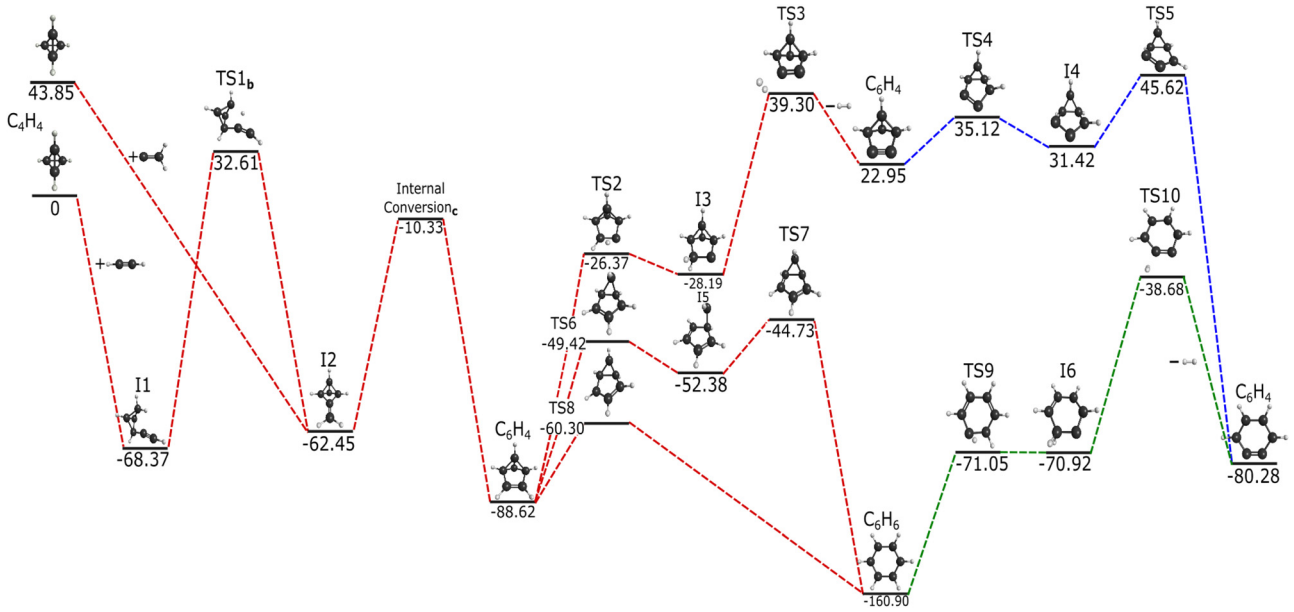

Fig. 5 Reaction pathway for the formation of *c*-C_6H_6 and *c*-C_6H_4 *via* HC≡CH and :CCH_2 addition to *c*-C_4H_4 in kcal mol^{-1}. TS1$_b$ represents the transition state analyzed in Fig. 6. Internal conversion$_c$ represents the intersection seen in Fig. 7. Red dashed lines represent this research, blue dashed lines are based on Poland *et al.*,[12] and green dashed lines are inspired from Kislov *et al.*[14]

3.3 HC≡CH and :CCH_2 addition to *c*-C_4H_4

The last pathway follows the inclusion of the isomers, :CCH_2 and HC≡CH, as separate reactants with *c*-C_4H_4, creating two interrelataed pathways. The reaction proceeds towards the creation of *c*-C_6H_6 and *c*-C_6H_4 shown in Fig. 5 largely with submerged barriers. Acetylene's previous detection in the IR within the ISM and vinylidene's potential existence implies that such a pathway may influence the interstellar production of benzene and *o*-benzyne and, hence, that of PAHs in the gas phase.

The addition of :CCH_2 to *c*-C_4H_4 leads to I2, which is a recognizable motif from the aforementioned intermediates of the previous reaction pathways. The inclusion of two hydrogens from the reactant separates this intermediate from the previous structures of similar connectivities. The creation of I2 from :CCH_2 and *c*-C_4H_4 allows for the formation of the cyclic C_6H_6 isomers and promotes stabilization from a diatomic hydrogen leaving group. While I2 can also be formed from acetylene combined with tetrahedrane, this reaction may be a non-starter as another step must take place before I2 is created.

HC≡CH reacting with *c*-C_4H_4 leads to I1 at −68.37 kcal mol^{-1}, which then requires an increase of 100.98 kcal mol^{-1} in order to reach the first transition state, lying at 32.61 kcal mol^{-1} above the reactants. This transition state, denoted as "TS1$_b$", is represented as the crossing point between the two potential energy curves seen in Fig. 6 with I1 and I2 as the minima. This scan follows the change in angle of the hydride shift from the bottom to the top-most carbon seen in I1 and I2. The point of crossing occurs at a bond angle of roughly 70° and serves as a maximum between the two intermediates, which interconvert *via* TS1$_b$. At this geometry the hydrogen migrates across two carbon atoms in a concerted motion according the

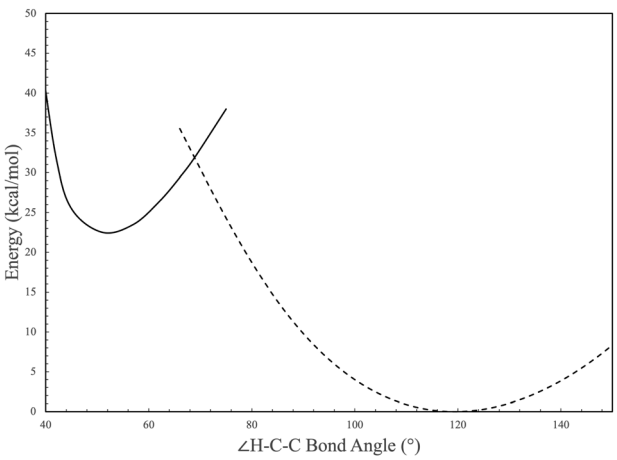

Fig. 6 Potential energy scan of H–C–C bond angle in TS1 of Fig. 5. Solid and dashed lines represent individual electronic states correlating to I2 and I1 in Fig. 5.

reaction coordinate and the imaginary frequency normal mode coordinate. However, the height of TS1$_b$ not only precludes the formation of I2 from acetylene and tetrahedrane, but it also keeps I1 from being created as any backwards pathways from I2. Hence, once I2 is made from :CCH_2 and *c*-C_4H_4, its most likely pathway is forward, away from either sets of reactants.

Consistent with the C_2H pathway, another internal conversion immediately after I2, denoted as "internal conversion$_c$" in Fig. 5, rests at −10.33 kcal mol^{-1} relative to acetylene or −54.18 kcal mol^{-1} relative vinylidene as the starting materials, and internal conversion$_c$ occurs between I2 and the *c*-C_6H_6 (benzvalene) isomer. In scanning across the bond distance defined from the mid point of the acetylene and a tetrahedrane

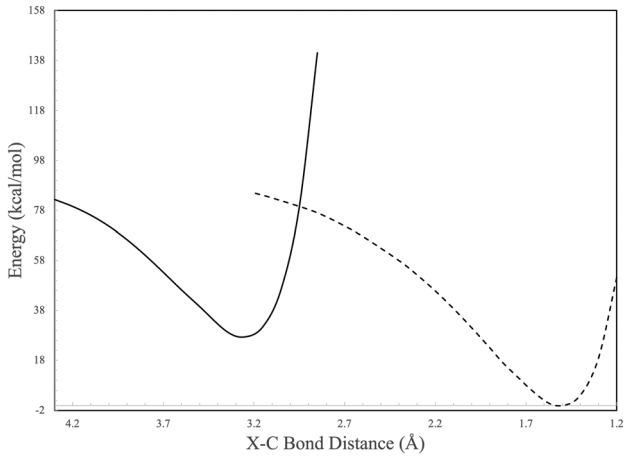

Fig. 7 Potential energy scan of X–C bond of HC≡CH and *c*-C_4H_4. Solid and dashed lines represent individual electronic states correlating to I2 and C_6H_6 in Fig. 5.

carbon vertex, two evident energetic wells (I2 and benzvalene) are formed and have their surfaces cross at an approximate bond length of 3.0 Å (Fig. 7). Subsequently, benzvalene sits at a minimum −88.62 kcal mol^{-1} below the reactants. Further analysis of internal conversion$_c$ showcases similar results as Fig. 4. At the geometries adjacent to the conversion maximum, the HOMO, HOMO−1, LUMO, and LUMO+1 retain their orbital symmetry and occupation as given in Fig. 8. The HOMO and the HOMO−1 switch positions between the two isomers as the carbon atoms from the two reactants interact with one another, but the orbital topologies are largely unchanged. This internal conversion is similar to that for the C_6H_5 PES described in the previous section but with the occupied orbitals shifting positions here. This produces the two minima shown in Fig. 7

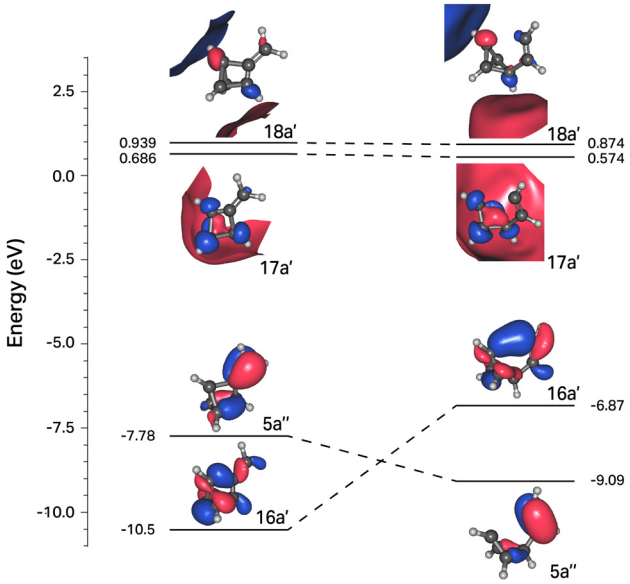

Fig. 8 Correlation diagram for the four frontier orbitals of structures to the right and left of the internal conversion shown in Fig. 7.

which correspond to I2 and benzvalene, respectively from left-to-right, and are given in their stations in Fig. 5.

Once benzvalene forms, it can then progress through three different isomerization pathways. The lower energy two have benzene as an intermediate, but all can lead to *o*-benzyne. The most energetically favorable pathway progresses through TS8 and then goes down significantly to benzene at −160.9 kcal mol^{-1}. TS6 is higher in energy and leads to I5 before a slight uphill to TS7 and onto benzene. TS6, TS7, and TS8 are all qualitatively similar, but the structures are slightly different with the five-member ring showing different puckering characteristics. However, the most notable difference are the normal coordinates for the imaginary frequencies. Regardless, the formation of benzene is energetically favorable and proceeds through these pinched six-membered rings. Formation of *o*-benzyne from benzene has been previously shown by Kislov *et al.*,[14] and this is verified here by more modern methods. I6 with two hydrogens on a single carbon is a minimum even with TS9 being very nearly degenerate. All materials lie below all starting materials, even TS10 before ushering off H_2 to generate *o*-benzyne.

The upper pathway from benzvalene to *o*-benzyne in Fig. 5 proceeds through TS2 and climbs up to TS3. This structure has an energy of −4.55 kcal mol^{-1} relative to vinylidene and tetrahedrane as the starting materials. Even if the acetylene reaction could produce I2, this pathway would not be energetically accessible. However, :CCH_2 as a reactant appears to be necessary to drive this reaction forward in the gas phase. TS3 loses H_2 at this step, and creates benzvalyne. The same process to produce *o*-benzyne as given in the C_6H_4 pathway is enacted, but TS5 here is 1.77 kcal mol^{-1} above even the :CCH_2 + *c*-C_4H_4 starting materials. However, ambient temperatures of 890 K would overcome this barrier, and even room temperature could get notable percentages (∼5%) of I4 to overcome the energy of TS5. Hence, even this upper pathway is not unreasonable but would require warm environments especially for astrochemical considerations.

4 Conclusions

In utilizing tetrahedrane as a stand-in for HTCs, this work shows that the reaction of vinylidene with HTCs can readily produce benzene, but benzene will likely only be an intermediate from this reaction since there is no leaving group in the reaction pathway. However, *o*-benzyne, a known interstellar molecule, could be formed in various pathways. Addition of the ethynyl radical to HTCs could also produce *o*-benzyne, but acetylene or C_2 reacting with HTCs likely will not. The former is due to energetics and the latter due to the lack of a leaving group to dissipate the excess energy kinetically. However, this work is showing that strained species can lead to other strained species before more stable molecules are produced. Such reactions certainly have applications to astrochemistry, and the possible interstellar observation of benzvalene or benzvalyne would certainly allow for more complicated organic

chemistry as shown in this work. In any case, reactions of HTCs, as modeled by tetrahedrane, with common, dicarbon molecules produce common, cyclic aromatic hydrocarbons as final products but also generate less well examined intermediates before doing so.

Author contributions

Taylor A. Cole: methodology, validation, formal analysis, investigation, data curation, writing – original draft, writing – review & editing, visualization. Steven R. Davis: conceptualization, methodology, validation, formal analysis, project administration, resources, software, supervision, writing – review & editing. Athena R. Flint: methodology, validation, formal analysis, investigation, writing – original draft, writing – review & editing, visualization. Ryan C. Fortenberry: conceptualization, methodology, validation, formal analysis, project administration, resources, software, supervision, writing – original draft, writing – review & editing, funding acquisition.

Conflicts of interest

There are no conflicts to declare.

Acknowledgements

The authors would like to thank funding from NASA Grants 22-A22ISFM-0009 & NNH22ZHA004C and from the University of Mississippi's College of Liberal Arts and Department of Chemistry. The computing resources utilized in this work were from the Mississippi Center for Supercomputing Research supported, in part, by NSF Grant OIA-1757220.

References

1 B. A. McGuire, A. M. Burkhardt, S. Kalenskii, C. N. Shingledecker, A. J. Remijan, E. Herbst and M. C. McCarthy, *Science*, 2018, **359**, 202–205.
2 B. A. McGuire, R. A. Loomis, A. M. Burkhardt, K. L. K. Lee, C. N. Shingledecker, S. B. Charnley, I. R. Cooke, M. A. Cordiner, E. Herbst, S. Kalenskii, M. A. Siebert, E. R. Willis, C. Xue, A. J. Remijan and M. C. McCarthy, *Science*, 2021, **371**, 1265.
3 C. Joblin and A. G. G. M. Tielens, *PAHs and the Universe*, EDP Sciences, 2011.
4 C. Shao, Q. Wang, W. Zhang, A. Bennett, Y. Li, J. Guo, H. G. Im, W. L. Roberts, A. Violi and S. M. Sarathy, *Commun. Chem.*, 2023, **6**, 223.
5 A. M. Burkhardt, K. L. K. Lee, P. B. Changala, C. N. Shingledecker, I. R. Cooke, R. A. Loomis, H. Wei, S. B. Charnley, E. Herbst, M. C. McCarthy and B. A. McGuire, *Astrophys. J., Lett.*, 2021, **913**, L18.
6 J. Cernicharo, M. Agúndez, R. I. Kaiser, C. Cabezas, B. Tercero, N. Marcelino, J. R. Pardo and P. de Vicente, *Astron. Astrophys.*, 2021, **652**, L9.
7 R. F. Knacke, *Nature*, 1977, **269**, 132–134.
8 M. Gatchell, J. Ameixa, M. Ji, M. H. Stockett, A. Simonsson, S. Denifl, H. Cederquist, H. T. Schmidt and H. Zettergren, *Nat. Commun.*, 2021, **12**, 6646.
9 J. Cernicharo, A. M. Heras, A. G. G. M. Tielens, J. R. Pardo, F. Herpin, M. Guélin and L. B. F. M. Waters, *Infrared Space Observatory's Discovery of C_4H_2, C_6H_2, and Benzene in CRL 618*, 2001.
10 E. F. van Dishoeck, S. Grant, B. Tabone, M. van Gelder, L. Francis, L. Tychoniec, G. Bettoni, A. M. Arabhavi, D. Gasman, P. Nazari, M. Vlasblom, P. Kavanagh, V. Christiaens, P. Klaassen, H. Beuther, T. Henning and I. Kamp, *Faraday Discuss.*, 2023, **245**, 52–79.
11 K. E. Wilzbach, J. S. Ritscher and L. Kaplan, *J. Am. Chem. Soc.*, 1967, **89**, 1031–1032.
12 K. N. Poland, W. Yang, R. C. Fortenberry and S. R. Davis, *Phys. Chem. Chem. Phys.*, 2022, **24**, 14573–14578.
13 K. N. Poland, B. R. Westbrook, D. H. Magers, R. C. Fortenberry and S. R. Davis, *J. Chem. Phys.*, 2022, **156**, 24302.
14 V. V. Kislov, T. L. Nguyen, A. M. Mebel, S. H. Lin and S. C. Smith, *J. Chem. Phys.*, 2004, **120**, 7008–7017.
15 H. Wang, A. Laskin, N. W. Moriarty and M. Frenklach, *On Unimolecular Decomposition of Phenyl Radical*, 2000.
16 A. Matsugi and A. Miyoshi, *Phys. Chem. Chem. Phys.*, 2012, **14**, 9722–9728.
17 A. Comandini and K. Brezinsky, *J. Phys. Chem. A*, 2012, **116**, 1183–1190.
18 C. W. Bauschlicher and A. Ricca, *Chem. Phys. Lett.*, 2013, **566**, 1–3.
19 L. V. Moskaleva, L. K. Madden and M. C. Lin, *Unimolecular isomerization/decomposition of ortho-benzyne: ab initio MO/statistical theory study*, 1999.
20 G. Ghigo, A. Maranzana and G. Tonachini, *Phys. Chem. Chem. Phys.*, 2014, **16**, 23944–23951.
21 S. P. Souza and B. L. Lutz, *Detection of C2 in the interstellar spectrum of Cygnus OB2 Number 12 (IV Cygni Number 12)*, 1977.
22 K. D. Tucker, M. L. Kutner and P. Thaddeus, *The Ethynyl Radical C2H-A New Interstellar Molecule*, 1974.
23 S. T. Ridgway, D. N. B. Hall, S. G. Kleinmann, D. A. Weinberger and R. S. Wojslaw, *Nature*, 1976, **264**, 345–346.
24 J. H. Lacy, N. J. Evans, J. M. Achtermann, D. E. Bruce, J. F. Arens and J. S. Carr, *Astrophys. J., Lett.*, 1989, **342**, L43.
25 J. M. Smith, M. Nikow, M. J. Wilhelm and H. L. Dai, *J. Phys. Chem. A*, 2023, **127**, 8782–8793.
26 J. Chang, L. Guo, R. Wang, J. Mou, H. Ren, J. Ma and H. Guo, *J. Phys. Chem. A*, 2019, **123**, 4232–4240.
27 R. L. Hayes, E. Fattal, N. Govind and E. A. Carter, *J. Am. Chem. Soc.*, 2001, **123**, 641–657.
28 R. I. Kaiser and N. Hansen, An Aromatic Universe-A Physical Chemistry Perspective, 2021.
29 F. C. Gillett, W. J. Forrest and K. M. Merrill, *Astrophys. J.*, 1973, **183**, 87.
30 A. G. G. M. Tielens, *Annu. Rev. Astron. Astrophys.*, 2008, **46**, 289–337.

31 E. Peeters, L. J. Allamandola, D. M. Hudgins, S. Hony and A. G. G. M. Tielens, *Astrophysics of Dust, ASP Conference Series*, Astronomical Society of the Pacific, San Francisco, CA, 2004, vol. 309, pp. 141–162.
32 E. Peeters, C. Mackie, A. Candian and A. G. G. M. Tielens, *Acc. Chem. Res.*, 2021, **54**, 1921–1933.
33 E. Peeters, S. Hony, C. Van Kerckhoven, A. G. G. M. Tielens, L. J. Allamandola, D. M. Hudgins and C. W. Bauschlicher, *Astron. Astrophys.*, 2002, **390**, 1089–1113.
34 E. Peeters, *Proceedings of the International Astronomical Union*, 2011, vol. 7, pp. 149-161.
35 G. C. Sloan, M. Jura, W. W. Duley, K. E. Kraemer, J. Bernard-Salas, W. J. Forrest, B. Sargent, A. Li, D. J. Barry, C. J. Bohac, D. M. Watson and J. R. Houck, *The Unusual Hydrocarbon Emission From the Early Carbon Star HD 100764: The Connection Between Aromatics and Aliphatics*, 2007.
36 L. D. Keller, G. C. Sloan, W. J. Forrest, S. Ayala, P. D'alessio, S. Shah, N. Calvet, J. Najita, A. Li, L. Hartmann, B. Sargent, D. M. Watson and C. H. Chen, *PAH Emission From Herbig Ae/Be Stars*, 2008.
37 M. S. Murga, S. A. Khoperskov and D. S. Wiebe, *Astron. Rep.*, 2016, **60**, 233–251.
38 B. Acke, J. Bouwman, A. Juhász, T. Henning, M. E. V. D. Ancker, G. Meeus, A. G. Tielens and L. B. Waters, *Astrophys. J.*, 2010, **718**, 558–574.
39 S. Kwok and Y. Zhang, *Nature*, 2011, **479**, 80–83.
40 T. P. Stecher, *Astrophys. J.*, 1965, **142**, 1683.
41 R. C. Bless and B. D. Savage, *Astrophys. J.*, 1972, **171**, 293.
42 T. Zafar, K. E. Heintz, J. P. U. Fynbo, D. Malesani, J. Bolmer, C. Ledoux, M. Arabsalmani, L. Kaper, S. Campana, R. L. C. Starling, J. Selsing, D. A. Kann, A. de Ugarte Postigo, T. Schweyer, L. Christensen, P. Møller, J. Japelj, D. Perley, N. R. Tanvir, P. DAvanzo, D. H. Hartmann, J. Hjorth, S. Covino, B. Sbarufatti, P. Jakobsson, L. Izzo, R. Salvaterra, V. DElia and D. Xu, *Astrophys. J.*, 2018, **860**, L21.
43 B. Draine, Interstellar Dust, 1989, p. 313.
44 B. Donn, *Astrophys. J., Lett.*, 1968, **152**, L129.
45 G. P. Vclovykin, *Interstellar Dust and Aromatic Carbon*, 1969.
46 X.-L. Sheng, Q.-B. Yan, F. Ye, Q.-R. Zheng and G. Su, *Phys. Rev. Lett.*, 2011, **106**, 155703.
47 P. M. W. Kalberla, W. B. Burton, D. Hartmann, E. M. Arnal, E. Bajaja, R. Morras and W. G. L. Pöppel, *The Leiden/Argentine/Bonn (LAB) Survey of Galactic HI: Final data release of the combined LDS and IAR surveys with improved stray-radiation corrections*, 2005.
48 P. M. Kalberla and J. Kerp, *Annu. Rev. Astron. Astrophys.*, 2009, **47**, 27–61.
49 V. J. Herrero, M. Jiménez-Redondo, R. J. Peláez, B. Maté and I. Tanarro, *Structure and evolution of interstellar carbonaceous dust. Insights from the laboratory*, 2022.
50 X. Y. Ma, Y. Y. Zhu, Q. B. Yan, J. Y. You and G. Su, *Mon. Not. R. Astron. Soc.*, 2020, **497**, 2190–2200.
51 P. E. Eaton and T. W. Cole, *J. Am. Chem. Soc.*, 1964, **86**, 3157–3158.
52 P. E. Eaton and T. W. Cole, *J. Am. Chem. Soc.*, 1964, **86**, 962–964.
53 L. A. Paquette, R. J. Ternansky, D. W. Balogh and G. Kentgen1, *Total Synthesis of Dodecahedrane*, 1983.
54 J. M. Schulman and T. J. Venanzi, *J. Am. Chem. Soc.*, 1974, **96**, 4739–4746.
55 Y. Ozaki, S. Saito, K.-I. Kondo, N. S. Zefirov, A. S. Koz'min and A. V. Abramenkov, *The Problem of Tetrahedrane The Problem of Tone Reproduction in Offset Lithography V G W Harrison-The Problem of Hydrostatic Pressure Generation using a Piston-Cylinder Device The Problem of Tetrahedrane*, 1978.
56 A. Nemirowski, H. P. Reisenauer and P. R. Schreiner, *Chem. – Eur. J.*, 2006, **12**, 7411–7420.
57 A. M. Mebel, V. V. KisIov and R. I. Kaiser, *J. Chem. Phys.*, 2006, **125**, 133113.
58 M. B. Gardner, B. R. Westbrook, R. C. Fortenberry and T. J. Lee, *Spectrochim. Acta, Part A*, 2021, **248**, 119184.
59 R. C. Fortenberry and T. J. Lee, in *Chapter Six - Computational vibrational spectroscopy for the detection of molecules in space*, ed. D. A. Dixon, Elsevier, 2019, vol. 15, pp. 173–202.
60 B. R. Westbrook, G. M. Beasley and R. C. Fortenberry, *Phys. Chem. Chem. Phys.*, 2022, **24**, 14348–14353.
61 F. Karagulian, C. A. Belis, C. F. C. Dora, A. M. Prüss-Ustün, S. Bonjour, H. Adair-Rohani and M. Amann, *Atmos. Environ.*, 2015, **120**, 475–483.
62 P. Pant and R. M. Harrison, *Atmos. Environ.*, 2013, **77**, 78–97.
63 U. Lohmann, F. Friebel, Z. A. Kanji, F. Mahrt, A. A. Mensah and D. Neubauer, *Nat. Geosci.*, 2020, **13**, 674–680.
64 M. Antiñolo, M. D. Willis, S. Zhou and J. P. D. Abbatt, *Nat. Commun.*, 2015, **6**, 6812.
65 H. Wang, *Proceedings of the Combustion Institute*, 2011, **33**, 41–67.
66 K. Raghavachari, G. W. Trucks, J. A. Pople and M. Head-Gordon, *A Fifth-Order Perturbation Comparison of Electron Correlation Theories*, 1989.
67 C. Hampel, K. A. Peterson and H.-J. Werner, *Chem. Phys. Lett.*, 1992, **190**, 1–12.
68 P. J. Knowles, C. Hampel and H.-J. Werner, *J. Chem. Phys.*, 1993, **99**, 5219–5227.
69 M. J. O. Deegan and P. J. Knowles, *Perturbative corrections to account for triple excitations in closed and open shell coupled cluster theories*, 1994.
70 T. D. Crawford and H. F. Schaefer III, *Rev. Comput. Chem.*, 2000, **14**, 33–136.
71 I. Shavitt and R. J. Bartlett, *Many-Body Methods in Chemistry and Physics: MBPT and Coupled-Cluster Theory*, Cambridge University Press, Cambridge, 2009.
72 T. H. Dunning, *J. Chem. Phys.*, 1989, **90**, 1007–1023.
73 K. A. Peterson and T. H. Dunning, *J. Chem. Phys.*, 1995, **102**, 2032–2041.
74 D. E. Woon and T. H. Dunning, *J. Chem. Phys.*, 1993, **98**, 1358–1371.
75 K. A. Peterson, T. B. Adler and H.-J. Werner, *J. Chem. Phys.*, 2008, **128**, 084102.

76 T. B. Adler, G. Knizia and H.-J. Werner, *J. Chem. Phys.*, 2007, **127**, 221106.
77 G. Knizia, T. B. Adler and H.-J. Werner, *J. Chem. Phys.*, 2009, **130**, 054104.
78 K. E. Yousaf and K. A. Peterson, *J. Chem. Phys.*, 2008, **129**, 184108.
79 J. G. Hill and K. A. Peterson, *Phys. Chem. Chem. Phys.*, 2010, **12**, 10460–10468.
80 W. Györffy and H.-J. Werner, *J. Chem. Phys.*, 2018, **148**, 114104.
81 H. J. Werner, P. J. Knowles, F. R. Manby, J. A. Black, K. Doll, A. Heßelmann, D. Kats, A. Köhn, T. Korona, D. A. Kreplin, Q. Ma, T. F. Miller, A. Mitrushchenkov, K. A. Peterson, I. Polyak, G. Rauhut and M. Sibaev, *J. Chem. Phys.*, 2020, **152**, 144107.
82 H.-J. Werner, P. J. Knowles, G. Knizia, F. R. Manby and M. Schütz, *Wiley Interdiscip. Rev.: Comput. Mol. Sci.*, 2012, **2**, 242–253.
83 H.-J. Werner and P. J. Knowles, *et al.*, *MOLPRO, version, a package of ab initio programs*, 2023.
84 A. D. Becke, *J. Chem. Phys.*, 1993, **98**, 5648–5652.
85 C. Lee, W. Yang and R. G. Parr, *Phys. Rev. B: Condens. Matter Mater. Phys.*, 1988, **37**, 785–789.
86 W. Yang, R. G. Parr and C. Lee, *Phys. Rev. A*, 1986, **34**, 4586–4590.
87 P. J. Stephens, F. J. Devlin, C. F. Chabalowski and M. J. Frisch, *J. Phys. Chem.*, 1994, **98**, 11623–11627.
88 S. H. Vosko, L. Wilk and M. Nusair, *Can. J. Phys.*, 1980, **58**, 1200–1211.
89 R. A. Kendall, T. H. Dunning and R. J. Harrison, *J. Chem. Phys.*, 1992, **96**, 6796–6806.
90 M. J. Frisch, G. W. Trucks, H. B. Schlegel, G. E. Scuseria, M. A. Robb, J. R. Cheeseman, G. Scalmani, V. Barone, G. A. Petersson, H. Nakatsuji, X. Li, M. Caricato, A. V. Marenich, J. Bloino, B. G. Janesko, R. Gomperts, B. Mennucci, H. P. Hratchian, J. V. Ortiz, A. F. Izmaylov, J. L. Sonnenberg, D. Williams-Young, F. Ding, F. Lipparini, F. Egidi, J. Goings, B. Peng, A. Petrone, T. Henderson, D. Ranasinghe, V. G. Zakrzewski, J. Gao, N. Rega, G. Zheng, W. Liang, M. Hada, M. Ehara, K. Toyota, R. Fukuda, J. Hasegawa, M. Ishida, T. Nakajima, Y. Honda, O. Kitao, H. Nakai, T. Vreven, K. Throssell, J. A. Montgomery, Jr., J. E. Peralta, F. Ogliaro, M. J. Bearpark, J. J. Heyd, E. N. Brothers, K. N. Kudin, V. N. Staroverov, T. A. Keith, R. Kobayashi, J. Normand, K. Raghavachari, A. P. Rendell, J. C. Burant, S. S. Iyengar, J. Tomasi, M. Cossi, J. M. Millam, M. Klene, C. Adamo, R. Cammi, J. W. Ochterski, R. L. Martin, K. Morokuma, O. Farkas, J. B. Foresman and D. J. Fox, *Gaussian~16 Revision C.01*, Gaussian Inc., Wallingford CT, 2016.
91 A. M. Turner, A. S. Koutsogiannis, N. F. Kleimeier, A. Bergantini, C. Zhu, R. C. Fortenberry and R. I. Kaiser, *Astrophys. J.*, 2020, **896**, 88.
92 A. M. Turner, S. Chandra, R. C. Fortenberry and R. I. Kaiser, *ChemPhysChem*, 2021, **22**, 985–994.
93 K. Fukui, *Acc. Chem. Res.*, 1981, **14**, 363–368.
94 A.-R. Allouche, *J. Comput. Chem.*, 2010, **32**, 174–182.
95 A. Allouche, *Gabedit*, 2017.
96 C. Puzzarini, *Front. Astron. Space Sci.*, 2022, **8**, 811342.
97 L. Tinacci, S. Ferrada-Chamorro, C. Ceccarelli, S. Pantaleone, D. Ascenzi, A. Maranzana, N. Balucani and P. Ugliengo, *Astrophys. J., Suppl. Ser.*, 2023, **266**, 38.
98 E. Herbst, *Front. Astron. Space Sci.*, 2021, **8**, 776942.
99 E. Hébrard, M. Dobrijevic, J. C. Loison, A. Bergeat, K. M. Hickson and F. Caralp, *Astron. Astrophys.*, 2013, **552**, A132.
100 R. C. Fortenberry, *Astrophys. J.*, 2021, **921**, 132.
101 A. Devaquet, *AVOIDED CROSSINGS IN PHOTOCHEMISTRY*.
102 A. Devaquet, A. Sevin and B. Bigot, *J. Am. Chem. Soc.*, 1978, **100**, 2009–2011.
103 S. Shaik, *J. Mol. Liq.*, 1994, **61**, 49–79.
104 L. Salem, C. Leforestier, G. Segal and R. Wetmore, *J. Am. Chem. Soc.*, 1975, **97**, 479–487.